

Thermonuclear Kinetics in Astrophysics

W. Raphael Hix^{a,b} Bradley S. Meyer^c

^a*Physics Division, Oak Ridge National Laboratory, Oak Ridge, TN 37831*

^b*Department of Physics & Astronomy, University of Tennessee, Knoxville, TN 37996*

^c*Department of Physics & Astronomy, Clemson University, Clemson, SC 29634*

Abstract

Over the billions of years since the Big Bang, the lives, deaths and afterlives of stars have enriched the Universe in the heavy elements that make up so much of ourselves and our world. This review summarizes the methods used to evolve these nuclear abundances within astrophysical simulations. These methods fall into 2 categories; evolution via rate equations and via equilibria. Because the rate equations in nucleosynthetic applications involve a wide range of timescales, implicit methods have proven mandatory, leading to the need to solve matrix equations. Efforts to improve the performance of such rate equation methods are focused on efficient solution of these matrix equations, in particular by making best use of the sparseness of these matrices, and finding methods that require less frequent matrix solutions. Recent work to produce hybrid schemes which use local equilibria to reduce the computational cost of the rate equations is also discussed. Such schemes offer significant improvements in the speed of reaction networks and are accurate under circumstances where calculations which assume complete equilibrium fail.

Key words: nucleosynthesis, numerical methods

PACS: 26.30.+k, 97.10.Cv, 95.75.Pq

1 Introduction

Research by Helmholtz, Kelvin and others throughout the second half of the 19th century made it clear that neither gravity nor any other then known energy source could account for the geologically determined age of the Sun and solar system. Enlightened by Rutherford's 1911 discovery of the atomic nucleus, Eddington and others suggested that nuclear transmutations might be the remedy to this quandary. With the burgeoning knowledge of the properties of nuclei and nuclear reactions in the 1930s, 1940s and 1950s came a

growing understanding of the role that individual nuclear reaction played in the synthesis of the elements. In 1957, Burbidge, Burbidge, Fowler & Hoyle [1] and Cameron [2] wove these threads into a cohesive theory of nucleosynthesis, and demonstrated how the solar isotopic abundances bore the fingerprints of their astrophysical origins. Today, investigations refine our answers to these same two questions; how are the elements we see on Earth and throughout the universe formed, and how do these nuclear transmutations, and the energy they release, affect their astrophysical hosts?

In this article, we will review the numerical methods used to study these questions. Two basic numerical methods are at the heart of the study of thermonuclear kinetics in astrophysics, the tracking of nuclear transmutations via rate equations and via equilibria. We will also briefly discuss work which seeks to meld these methods together in order to overcome the limitations of each. Additionally we will discuss the issues encountered when coupling the nuclear evolution to hydrodynamic simulations.

2 Thermonuclear Reaction Networks

Composed of a system of first order differential equations, the nuclear reaction network has sink and source terms representing each of the many nuclear reactions involved. Prior to discussing the numerical difficulties posed by the nuclear reaction network, it is necessary to understand the sets of equations we are attempting to solve. To this end, we present a brief overview of the thermonuclear reaction rates of interest and how these rates are assembled into the differential equations that must ultimately be solved. For more detailed information, we refer the reader to several textbooks covering this subjects [3,4,5]. We will end this section by briefly discussing the coupling of nucleosynthesis with hydrodynamics.

2.1 *Thermonuclear Reaction Rates*

There are a large number of types of nuclear reactions which are of astrophysical interest. In addition to the emission or absorption of nuclei and nucleons, nuclear reactions can involve the emission or absorption of photons (γ -rays) and leptons (electrons, neutrinos, and their anti-particles). As a result, nuclear reactions involve three of the four fundamental forces, the nuclear strong, electromagnetic and nuclear weak forces. Reactions involving leptons (termed weak interactions) proceed much more slowly than those involving only nucleons and photons; however, these reactions are important because only weak interactions can change the global ratio of protons to neutrons.

The most basic piece of information about any nuclear reaction is the nuclear cross section. The cross section for a reaction between target j and projectile k is defined by

$$\sigma = \frac{\text{number of reactions target}^{-1}\text{sec}^{-1}}{\text{flux of incoming projectiles}} = \frac{r/n_j}{n_k v}. \quad (1)$$

The second equality holds when the relative velocity between targets of number density n_j and projectiles of number density n_k is constant and has the value v . Then r , the number of reactions per cm^3 and sec, can be expressed as $r = \sigma v n_j n_k$. More generally, the targets and projectiles have distributions of velocities, in which case r is given by

$$r_{j,k} = \int \sigma(|\vec{v}_j - \vec{v}_k|) |\vec{v}_j - \vec{v}_k| d^3 n_j d^3 n_k. \quad (2)$$

The evaluation of this integral depends on the types of particles and distributions which are involved. For nuclei j and k in an astrophysical plasma, Maxwell-Boltzmann statistics generally apply; thus,

$$d^3 n = n \left(\frac{m}{2\pi k_B T} \right)^{3/2} \exp\left(-\frac{mv^2}{2k_B T}\right) d^3 v, \quad (3)$$

allowing n_j and n_k to be moved outside of the integral. Eq. 2 can then be written as $r_{j,k} = \langle \sigma v \rangle_{j,k} n_j n_k$, where $\langle \sigma v \rangle$ is the velocity integrated cross section. Equivalently, one can express the reaction rate in terms of a mean lifetime of particle j against destruction by particle k ,

$$\tau_k(j) = \frac{1}{\langle \sigma v \rangle_{j,k} n_k} \quad (4)$$

For thermonuclear reactions, these integrated cross sections have the form [3,6]

$$\langle j, k \rangle \equiv \langle \sigma v \rangle_{j,k} = \left(\frac{8}{\mu\pi} \right)^{1/2} (k_B T)^{-3/2} \int_0^\infty E \sigma(E) \exp(-E/k_B T) dE, \quad (5)$$

where μ denotes the reduced mass of the target-projectile system, E the center of mass energy, T the temperature and k_B is Boltzmann's constant.

Experimental measurements and theoretical predictions for these reaction rates provide the data input necessary to study astrophysical thermonuclear kinetics. While detailed discussion of individual rates is beyond the scope of this article, the interested reader is directed to the following reviews, in this

volume and elsewhere. Experimental nuclear rates and the methodology for measuring them have been reviewed in detail by [4,7]. A number of articles in this volume review the charged particle reaction rates which are important in the Sun [8], in later stages of stellar evolution [9], and for explosive burning on compact objects [10,11,12]. Experimental neutron capture cross sections are also summarized [13,14]. Theoretical modeling of these rates [15,16] is vitally important to provide the many rates for which experimental information is incomplete or non-existent. Beyond measuring or calculating these rates, progress in nuclear astrophysics also requires the compilation and dissemination (in a usable form) of this hard-earned nuclear data to the broadest astrophysical community [17,18,19].

When particle k in Eq. 2 is a photon, the distribution d^3n_k is given by the Plank distribution. Furthermore, the relative velocity is always c and thus the integral is separable, simplifying to

$$r_j = \frac{\int d^3n_j}{\pi^2(c\hbar)^3} \int_0^\infty \frac{c\sigma(E_\gamma)E_\gamma^2}{\exp(E_\gamma/k_B T) - 1} dE_\gamma \equiv \lambda_{j,\gamma}(T)n_j. \quad (6)$$

In practice it is not usually necessary to directly evaluate the photodisintegration cross sections (see, however, [20] for exceptions), because they can be expressed by detailed balance in terms of the capture cross sections for the inverse reaction, $l + m \rightarrow j + \gamma$ [6].

$$\lambda_{j,\gamma}(T) = \left(\frac{G_l G_m}{G_j}\right) \left(\frac{A_l A_m}{A_j}\right)^{3/2} \left(\frac{m_u k_B T}{2\pi\hbar^2}\right)^{3/2} \langle l, m \rangle \exp(-Q_{lm}/k_B T). \quad (7)$$

This expression depends on the partition functions, $G_k = \sum_i (2J_i + 1) \exp(-E_i/k_B T)$ (which account for the populations of the excited states of the nucleus), the mass numbers, A , the temperature T , the inverse reaction rate $\langle l, m \rangle$, and the reaction Q -value (the energy released by the reaction), $Q_{lm} = (m_l + m_m - m_j)c^2$. Since photodisintegrations are endoergic, their rates are vanishingly small until sufficient photons exist in the high energy tail of the Planck distribution with energies $> Q_{lm}$. As a rule of thumb this requires $T \approx Q_{lm}/30k_B$.

In practice, these experimental and theoretical reaction rates are determined for bare nuclei, while in astrophysical plasmas, these reactions occur among a background of other nuclei and electrons. As a result of this background, the reacting nuclei experience a Coulomb repulsion modified from that of bare nuclei. For high densities and/or low temperatures, the effects of this screening of reactions becomes very important. Under most conditions (with non-vanishing temperatures) the generalized reaction rate integral can be separated into the

traditional expression without screening [Eq. 5] and a screening factor,

$$\langle j, k \rangle^* = f_{scr}(Z_j, Z_k, \rho, T, n_i) \langle j, k \rangle. \quad (8)$$

This screening factor is dependent on the charge of the involved particles, the density, temperature, and the composition of the plasma. For more details on the form of f_{scr} , see, e.g., [21,22,23,24]. At high densities and low temperatures screening factors can enhance reactions by many orders of magnitude and lead to *pycnonuclear ignition*. In the extreme case of very low temperatures, where reactions are only possible via ground state oscillations of the nuclei in a Coulomb lattice, Eq. 8 breaks down, because it was derived under the assumption of a Boltzmann distribution [25,26].

In stellar plasmas, target nuclei also do not exist solely in their ground states. This complicates the rate expression in Eq. 5, which now must take into account the cross sections for capture out of the different excited states and properly weight them according to their probability of occurrence in the ensemble of target nuclei. Because the timescales for transitions between excited states of a nucleus are typically much shorter than other reaction timescales, it is usually valid to assume that the nuclei are internally equilibrated and a given excited state is populated in the ensemble by the usual Boltzmann factor $\propto e^{-E/k_B T}$, where E now is the excitation energy of that state. From this, one may derive a factor, called the *stellar enhancement factor* (SEF), to correct the ground-state reaction rate for the population of excited states (see, e.g., [27,28]).

Interesting complications to this prescription arise when the internal equilibration timescale for a nucleus exceeds the other reaction timescales in the problem. This usually occurs when a large spin difference between the ground state of an isotope and its first excited state prevents them from communicating directly via internal transitions. The isotope ^{26}Al is the prototypical example, with a ground and isomeric state of spin and parity 5^+ and 0^+ , respectively. When these two states equilibrate, it is not through a direct transition between the states—that simply takes too long. Rather the equilibration occurs through transitions to higher-lying levels that communicate effectively with both levels. This problem has been studied in detail (e.g., [29]), and the most straightforward way of dealing with this is to assume that the higher-lying levels are in a steady state since their destruction timescales are so rapid. When this is done, the population of the target nucleus break up into two ensembles, one tied to the ground state and one tied to the isomer [30]. These may then be treated as separate species in the network, each with its own rates to and from other isotopes and with effective rates for transitions between the two ensembles. Fortunately, the number of nuclei requiring such treatment is small and does not add much computational burden to running the nuclear reaction network.

A procedure similar to that used to derive Eq. 6 applies to captures of electrons by nuclei. Because the electron is 1836 times less massive than a nucleon, the velocity of the nucleus j in the center of mass system is negligible in comparison to the electron velocity ($|\vec{v}_j - \vec{v}_e| \approx |\vec{v}_e|$). In the neutral, completely ionized plasmas typical of the astrophysical sites of nucleosynthesis, the electron number density, n_e , is equal to the total density of protons in nuclei, $\sum_i Z_i n_i$. However in many of these astrophysical settings the electrons are at least partially degenerate, therefore the electron distribution cannot be assumed to be Maxwellian. Instead the capture cross section may be integrated over a Boltzmann, partially degenerate, or degenerate Fermi distribution of electrons, depending on the astrophysical conditions. The resulting electron capture rates are functions of T and n_e , $r_j = \lambda_{j,e}(T, n_e)n_j$. Similar equations apply for the capture of positrons which are in thermal equilibrium with photons, electrons, and nuclei. Electron and positron capture calculations have been performed for a large variety of nuclei with mass numbers between $A=20$ and $A=100$ (see [31] for more information). For normal decays, like beta or alpha decays, with a characteristic half-life $\tau_{1/2}$, Eq. 6 also applies, with the decay constant $\lambda_j = \ln 2/\tau_{1/2}$. In addition to innumerable experimental half-life determinations, beta-decay half-lives for a wide range of unstable nuclei have been predicted (see [32,33]).

Even though the size of the neutrino scattering cross section on nuclei and electrons is very small, at high densities ($\rho \sim 10^{13} \text{ g cm}^{-3}$), enough scattering events occur to thermalize the neutrino distribution. Under such conditions the inverse process to electron capture (neutrino capture) can occur in significant numbers and the neutrino capture rate can be expressed in a form similar to Eqs. 6 by integrating over the thermal neutrino distribution (e.g. [34]). Inelastic neutrino scattering on nuclei can also be expressed in this form. The latter can cause particle emission, similar to photodisintegration. In this volume, see [35,36,37] for more complete discussion of the interactions of neutrinos with matter. The calculation of these rates can be further complicated by the neutrinos being out of thermal equilibrium with the local environment. When thermal equilibrium among neutrinos was established at a different location, then the neutrino distribution might be characterized by a chemical potential and a temperature different from the local values. Otherwise, the neutrino distribution must be evolved in detail (see, e.g., [38]).

2.2 *Thermonuclear Rate Equations*

The large number of reaction types discussed in §2.1 can be divided into 3 functional categories based on the number of reactants which are nuclei. The reactions involving a single nucleus, which include decays, electron and positron captures, photodisintegrations, and neutrino induced reactions, de-

pend on the number density of only the target species. For reaction involving two nuclei, the reaction rate depends on the number densities of both target and projectile nuclei. There are also a few important three-particle process (like the triple- α process, see §5) which are commonly successive captures with an intermediate unstable target (see, e.g., [39,40]). Using an equilibrium abundance for the unstable intermediate, the contributions of these reactions are commonly written in the form of a three-particle processes, depending on a trio of number densities. Grouping reactions by these 3 functional categories, the time derivatives of the number densities of each nuclear species in an astrophysical plasma can be written in terms of the reaction rates, r , as

$$\left. \frac{\partial n_i}{\partial t} \right|_{\rho=const} = \sum_j \mathcal{N}_j^i r_j + \sum_{j,k} \mathcal{N}_{j,k}^i r_{j,k} + \sum_{j,k,l} \mathcal{N}_{j,k,l}^i r_{j,k,l}, \quad (9)$$

where the three sums are over reactions which produce or destroy a nucleus of species i with 1, 2 & 3 reactant nuclei, respectively. The \mathcal{N} s provide for proper accounting of numbers of nuclei and are given by: $\mathcal{N}_j^i = N_i$, $\mathcal{N}_{j,k}^i = N_i / \prod_{m=1}^{n_{j,k}} |N_m|!$, and $\mathcal{N}_{j,k,l}^i = N_i / \prod_{m=1}^{n_{j,k,l}} |N_m|!$. The N_i 's can be positive or negative numbers that specify how many particles of species i are created or destroyed in a reaction, while the denominators, including factorials, run over the $n_{j,k}$ or $n_{j,k,l}$ different species destroyed in the reaction and avoid double counting of the number of reactions when identical particles react with each other (for example in the $^{12}\text{C} + ^{12}\text{C}$ or the triple- α reactions; for details see [6]).

In addition to nuclear reactions, expansion or contraction of the plasma can also produce changes in the number densities n_i . To separate the nuclear changes in composition from these hydrodynamic effects, the nuclear abundance $Y_i = n_i / \rho N_A$, where N_A is Avogadro's number, is commonly used. For a nucleus with atomic weight A_i , $A_i Y_i$ represents the mass fraction of this nucleus, therefore $\sum A_i Y_i = 1$. Likewise, the equation of charge conservation becomes $\sum Z_i Y_i = Y_e$, where $Y_e (= n_e / \rho N_A)$ is the electron abundance (also termed the electron fraction). By recasting Eq. 9 in terms of nuclear abundances Y_i , a set of ordinary differential equations for the evolution of Y_i results which depends only on nuclear reactions. In terms of the reaction cross sections introduced in §2.1, this reaction network is described by the following set of differential equations

$$\dot{Y}_i = \sum_j \mathcal{N}_j^i \lambda_j Y_j + \sum_{j,k} \mathcal{N}_{j,k}^i \rho N_A \langle j, k \rangle Y_j Y_k + \sum_{j,k,l} \mathcal{N}_{j,k,l}^i \rho^2 N_A^2 \langle j, k, l \rangle Y_j Y_k Y_l. \quad (10)$$

2.3 Coupling Nuclear Reaction Networks to Hydrodynamics

As we touched on in the previous section, nuclear processes are tightly linked to the hydrodynamic behavior of the bulk medium. Thermonuclear processes release (or absorb) energy, which alters the pressure and causes hydrodynamic motions. These motions may disperse the thermonuclear ash and bring a continued supply of fuel to support the thermonuclear flame. The compositional changes caused by thermonuclear reactions can also change the equation of state and opacity, further impacting the hydrodynamic behavior. For purposes of this review of thermonuclear kinetics methods, which generally assume that thermonuclear and hydrodynamic changes in local composition can be successfully decoupled (or treated in an operator split fashion), we include only a brief description of how this decoupling is best achieved. Müller [41] provides an authoritative overview and discusses the difficulties (and open issues) involved when including nucleosynthesis within hydrodynamic simulations.

The coupling between thermonuclear processes and hydrodynamic changes can be divided into two categories by considering the spatial extent of the coupling. Nucleosynthetic changes in composition and the resultant energy release produce *local* changes in hydrodynamic quantities like pressure and temperature. The strongest of these local couplings is the release (or absorption) of energy and the resultant change in temperature. Changes in temperature are particularly important because of the exponential nature of the temperature dependence of thermonuclear reaction rates. Since the nuclear energy release is uniquely determined by the abundance changes, the rate of thermonuclear energy release, $\dot{\epsilon}$, is given by

$$\dot{\epsilon}_{nuc} = - \sum_i N_A M_i c^2 \dot{Y}_i \text{ (MeV g}^{-1} \text{ s}^{-1}\text{)}. \quad (11)$$

where $M_i c^2$ is the rest mass energy of species i in MeV. Since all reactions conserve nucleon number, the atomic mass excess $M_{ex,i} = M_i - A_i m_u$ (m_u is the atomic mass unit) can be used in place of the mass M_i in Eq. 11 (see [42] for a recent compilation of mass excesses). The use of atomic mass units has the added benefit that electron conservation is correctly accounted for in the case of β^- decays and e^- captures, though reactions involving positrons require careful treatment. In general, the nuclear energy release is deposited locally, so the rate of thermonuclear energy release is equal to the nuclear portion of the hydrodynamic heating rate. However, there are instances where nuclear products do not deposit their energy locally. Escaping neutrinos can carry away a portion of the thermonuclear energy release. In the rarefied environment of supernova ejecta at late times, positrons and gamma rays released by β decays are not completely trapped. In most such cases, the escaping particles stream freely from the reaction site, allowing adoption of a simple loss term

analogous to Eq. 11 with $M_i c^2$ replaced by an averaged energy loss term. For this reason, weak reaction rate tabulations provide averaged neutrino losses. From these we can construct

$$\dot{\epsilon}_{\nu \text{ loss}} = \sum_i \langle E_\nu \rangle \dot{Y}_{i, \text{weak}}, \quad (12)$$

where we consider only those contributions to \dot{Y} due to neutrino producing reactions. In some cases, like supernovae, subsequent interactions between the escaping leptons or gamma rays and matter require more complete transport to be considered. Other important quantities which are impacted by nucleosynthesis, like Y_e , can be obtained by appropriate sums over the abundances and also need not be evolved separately.

Implicit solution methods require the calculation of $\dot{Y}(t + \Delta t)$, where Δt is the nuclear timestep, which in turn requires knowledge of $T(t + \Delta t)$. One could write a differential equation for the energy release analogous to Eq. 10, with the \mathcal{N} s replaced by the reaction Q -values, and thereby evolve the energy release (and calculate temperature changes) as an additional equation within the network solution. Müller [44] has shown that such a scheme can help avoid instabilities in the case of a physically isolated zone entering or leaving nuclear statistical equilibrium. In general, however, use of this additional equation is made unnecessary by the relative slowness with which the temperature changes. The timescale on which the temperature changes is given by

$$\tau_T = T/\dot{T} \approx C_V T / \dot{\epsilon}_{nuc} \quad (13)$$

and is often called the *ignition timescale*. The timescale on which an individual abundance changes is its *burning time*,

$$\tau(^A Z) = Y(^A Z) / \dot{Y}(^A Z) \sim \min_k \tau_k(^A Z) \quad (14)$$

where $\tau_k(^A Z)$ is defined in Eq. 4. In general τ_T differs from $\tau(^A Z)$ of the principle fuel by the ratio of thermal energy content to the energy released by the reaction. For degenerate matter this ratio can approach zero, allowing for explosive burning. In contrast, accurate prediction of less abundant, but still important, species requires that the reaction network timestep Δt be chosen to be the burning timescale of a less abundant species, typically with an abundance of 10^{-6} or smaller [45]. Since the dominant fuel is most often one of the more abundant constituents and the burning timescales are proportional to the abundance, τ_T is typically an order of magnitude or more larger than the reaction network timestep (see, e.g., [46,47]). It is therefore sufficient to calculate the energy gain at the end of a timestep via equation 11, modified as discussed above, and approximate $T(t + \delta t) \approx T(t)$ or to extrapolate based

on $\dot{\epsilon}(t)$. Since other locally coupled quantities have characteristic timescales much longer than Δt , they too can be decoupled in a similar fashion. For the remainder of this review, we will consider only the equations governing changes in isotopic abundances, remembering that additional equations can easily be constructed for those special circumstances where they are necessary.

Spatial coupling, particularly the modification of the composition by hydrodynamic movements such as diffusion, convective mixing and advection (in the case of Eulerian hydrodynamics methods), represents a more difficult challenge. By necessity, an individual nucleosynthesis calculation examines the abundance changes in a locality of uniform composition. The difficulties associated with strong spatial coupling of the composition occur because this nucleosynthetic calculation is spread over an entire hydrodynamic zone. Convection can result in strong abundance gradients across a single hydrodynamic zone, which with the assumption of compositional uniformity, can result in very different outcomes as a function of the fineness of the hydrodynamic grid. Thermonuclear supernovae, where the thickness of the flame front can be billionths of the radius of the white dwarf [48,49], present an extreme example of microscopic nuclear inhomogeneity. Eulerian advection of compositional boundaries can also have extremely unphysical consequences. Fryxell et al. [50] demonstrated how this artificial mixing can produce an unphysical detonation in a shock tube calculation by mixing cold unburnt fuel into the hot burnt region. A related problem is the conservation of species. Hydrodynamic schemes must carefully conserve the abundances (or partial densities) of all species [50,51,52], lest they provide unphysical abundances to the nucleosynthesis calculations, which must assume conservation, and thereby produce unphysical results. Because of these problems, hydrodynamic methods with excellent capture of shocks and contact or compositional discontinuities are best suited to nucleosynthesis calculations.

The relative size of the burning timescales, when compared to the relevant diffusion, sound crossing or convective timescale, dictates how these problems must be addressed. If all of the burning timescales are much shorter than the timescale on which the hydrodynamics changes the composition, then the assumption of uniform composition is satisfied and the nucleosynthesis of each hydrodynamic zone can be treated independently. If all of the burning timescales are much larger than, for example, the convective timescale, then the composition of the entire convective zone can be treated as uniform and slowly evolving. The greatest complexity occurs when the timescales on which the hydrodynamics and nucleosynthesis change the composition are similar. Oxygen shell burning represents an excellent example of this as the sound travel, convective turnover and nuclear burning timescales are all of the same order as the evolutionary time. The results of 2D simulations [53] demonstrate convective overshooting, highly non-uniform burning and a velocity structure dominated by convective plumes. In section 3.1 we will briefly discuss the nu-

merical challenges posed by fully coupling nucleosynthesis and nuclear mixing. Silicon burning represents a different challenge [5], as the timescales for the transformation of silicon to iron are much slower than the convective turnover time, but the burning timescales for the free neutrons, protons and α -particles which maintain QSE are much faster, providing a strong motivation for the hybrid reaction networks we will discuss in §5.

3 Solving the Nuclear Reaction Network

In principle, the initial value problem presented by the nuclear reaction network can be solved by any of a large number of methods discussed in the literature. However the physical nature of the problem, reflected in the λ 's and $\langle\sigma v\rangle$'s, greatly restricts the optimal choice. The large number of reactions display a wide range of reaction timescales, τ (see Eq. 4). Numerical systems whose solutions depend on a wide range of timescales are termed *stiff*. Gear [54] demonstrated that even a single equation can be stiff if it has both rapidly and slowly varying components. Practically, stiffness occurs when the limitation of the timestep size is due to numerical stability rather than accuracy. A more rigorous definition [55] is that a system of equations $\vec{Y}(\vec{Y})$ is stiff if the eigenvalues λ_j of the Jacobian $\partial\vec{Y}/\partial\vec{Y}$ obey the criterion that for negative $\Re(\lambda_j)$ (the real part of the eigenvalues λ_j)

$$\mathcal{S} = \frac{\max|\Re(\lambda_j)|}{\min|\Re(\lambda_j)|} \gg 1 \quad (15)$$

for $j = 1, \dots, N$. As we will explain in this section, $\mathcal{S} > 10^{15}$ is not uncommon in astrophysics.

Astrophysical calculations of nucleosynthesis belong to the general field of reactive flows, and therefore share some characteristics with related terrestrial fields. In particular, chemical kinetics, the study of the evolution of chemical abundances, is an important part of atmospheric and combustion physics and produces sets of equations much like Eq. 9 (see [56] for a thorough introduction). These chemical kinetics systems are known for their stiffness and a great deal of effort has been expended on developing methods to solve these equations. Many of the considerations for the choice of solution method for chemical kinetics also apply to thermonuclear kinetics. In both cases, temporal integration of the reaction rate equations is broken up into short intervals because of the need to update the hydrodynamics variables. This favors one step, self starting algorithms. Because abundances must be tracked for a large number of computational cells (hundreds to thousands for one dimensional models, millions to billions for the coming generation of three dimensional models),

memory storage concerns favor low order methods since they don't require the storage of as much data from prior steps. In any event, both the errors in fluid dynamics and in the reaction rates are typically a few percent or more, so the greater precision of these higher order methods often does not result in greater accuracy. Note that these statements do not in general apply to calculations of Big Bang nucleosynthesis (at least those that assume homogeneity). As a result quite different methods are employed in these calculations [57]

Because of the wide range in timescales between strong, electromagnetic and weak reactions, nuclear reaction networks are extraordinarily stiff. PP chain nucleosynthesis, responsible for the energy output of the Sun, offers an excellent example of the difficulties. The first reaction of the PP1 chain is ${}^1\text{H}(p, e^+\nu){}^2\text{H}$, the fusion of two protons to form deuterium. This is a weak reaction, requiring the conversion of a proton into a neutron, and releasing a positron and a neutrino. As a result, the reaction timescale $\tau_p({}^1\text{H})$ is very long, billions of years for conditions like those in the solar interior. The second reaction of the PP1 chain is the capture of a proton on the newly formed deuteron, ${}^2\text{H}(p, \gamma){}^3\text{He}$. For conditions like those in the solar interior, the characteristic timescale, $\tau_p({}^2\text{H})$ is a few seconds. Thus the timescales for two of the most important reactions for hydrogen burning in stars like our Sun differ by more than 17 orders of magnitude (see [3,8] for a more complete discussion of the PP chain). This disparity results not from a lack of ${}^1\text{H} + {}^1\text{H}$ collisions (which occur at a rate $Y({}^1\text{H})/Y({}^2\text{H}) \sim 10^{17}$ times more often than ${}^1\text{H} + {}^2\text{H}$ collisions), but from the rarity of the transformation of a proton to a neutron. While the presence of weak reactions among the dominant energy producing reactions is unique to hydrogen burning, most nucleosynthesis calculations are similarly stiff, in part because of the need to include weak interactions but also the potential for neutron capture reactions, which occur very rapidly even at low temperature, following any release of free neutrons. The nature of the nuclear reaction network equations has thus far limited the astrophysical usefulness of the most sophisticated methods to solve stiff equations developed for chemical kinetics. However work to harness this resource continues. For example, Timmes [58] has examined higher order Kaps-Rentrop and Bader-Deuffhard semi-implicit time integration algorithms while Mott et al. [59] have studied asymptotic and quasi-steady state methods, which do not require a matrix solution.

For a set of nuclear abundances \vec{Y} , one can calculate the time derivatives of the abundances, $\dot{\vec{Y}}$ using Eq. 10. The desired solution is the abundance at a future time, $\vec{Y}(t + \Delta t)$, where Δt is the network timestep. For simplicity, most past and present nucleosynthesis calculations use the simple finite difference prescription

$$\frac{\vec{Y}(t + \Delta t) - \vec{Y}(t)}{\Delta t} = (1 - \Theta)\dot{\vec{Y}}(t + \Delta t) + \Theta\dot{\vec{Y}}(t). \quad (16)$$

This choice is also supported by the advantages of coupling low order, single step methods with hydrodynamics. With $\Theta = 1$, Eq. 16 becomes the explicit Euler method while for $\Theta = 0$ it is the implicit backward Euler method, both of which are first order accurate. For $\Theta = 1/2$, Eq. 16 is the semi-implicit trapezoidal method, which is second order accurate. For the stiff set of non-linear differential equations which form most nuclear reaction networks, a fully implicit treatment is generally most successful [45], though the trapezoidal method has been used in Big Bang nucleosynthesis calculations [60], where coupling to hydrodynamics is less important. Solving the fully implicit version of Eq. 16 is equivalent to finding the zeros of the set of equations

$$\vec{\mathcal{Z}}(t + \Delta t) \equiv \frac{\vec{Y}(t + \Delta t) - \vec{Y}(t)}{\Delta t} - \dot{\vec{Y}}(t + \Delta t) = 0 . \quad (17)$$

This is done using the Newton-Raphson method (see, e.g., [61]), which is based on the Taylor series expansion of $\vec{\mathcal{Z}}(t + \Delta t)$, with the trial change in abundances given by

$$\Delta \vec{Y} = \left(\frac{\partial \vec{\mathcal{Z}}(t + \Delta t)}{\partial \vec{Y}(t + \Delta t)} \right)^{-1} \vec{\mathcal{Z}} , \quad (18)$$

where $\partial \vec{\mathcal{Z}} / \partial \vec{Y}$ is the Jacobian of $\vec{\mathcal{Z}}$.

Historically [45] and in some modern applications (see, e.g., [62]), each timestep consists of only a single application of the procedure outlined in Eqs. 17 & 18. This semi-implicit backward Euler method has the advantage of a relatively small and predictable number of matrix solutions, but there are only heuristic checks that the chosen timestep results in a stable or accurate solution. In fully implicit backward Euler schemes, iteration using the procedure of Eqs. 17 & 18 continues until both $\Delta \vec{Y}$ and $\vec{\mathcal{Z}}$ are below some tolerance, providing a measure of the stability and accuracy. If this convergence does not occur within a reasonable number of iterations, the timestep is subdivided into smaller intervals until a converged solution can be achieved, allowing the fully implicit backward Euler integration to respond to instability or inaccuracy in a way that is impossible with the semi-implicit backward Euler approach. Higher order methods allow better estimates of the truncation error by comparing the solutions of different order schemes and sub-dividing the timestep if these errors are too large.

A potential numerical problem with the solution of Eq. 17 is the singularity of the Jacobian matrix, $\partial \vec{\mathcal{Z}}(t + \Delta t) / \partial \vec{Y}(t + \Delta t)$. From Eq. 17, the individual

matrix elements of the Jacobian have the form

$$\frac{\partial Z_i}{\partial Y_j} = \frac{\delta_{ij}}{\Delta t} - \frac{\partial \dot{Y}_i}{\partial Y_j} = \frac{\delta_{ij}}{\Delta t} - \sum \frac{1}{\tau_j(i)}, \quad (19)$$

where δ_{ij} is the Kronecker delta, and $\tau_j(i)$ is the destruction timescale of nucleus i with respect to nucleus j for a given reaction, as defined in Eq. 4. The sum accounts for the fact that there may be more than one reaction by which nucleus j is involved in the creation or destruction of nucleus i . Along the diagonal of the Jacobian, there are two competing terms, $1/\Delta t$ and $\sum 1/\tau_i(i)$. This sum is over all reactions which destroy nucleus i , and is dominated by the fastest reactions. As a result, $\sum 1/\tau_i(i)$ can be orders of magnitude larger than the reciprocal of the desired timestep, $1/\Delta t$. This is especially a problem near equilibrium, where both destruction and the balancing production timescales are very short in comparison to the preferred timestep size, resulting in differences close to the numerical accuracy (i.e. 14 or more orders of magnitude). In such cases, the term $1/\Delta t$ is numerically neglected, leading to numerically singular matrices. One approach to avoiding this problem is to artificially scale these short, equilibrium timescales by a factor which brings their timescale closer to Δt , but leaves them small enough to ensure equilibrium. While this approach has been used successfully, the ad hoc nature of this artificial scaling renders these methods fragile. A more promising approach is to make directly use of equilibrium expressions for abundances, which, as we will discuss in §5, also ensures the economical use of computer resources.

3.1 Taking Advantage of Matrix Sparseness

For larger nuclear reaction networks, the Newton-Raphson method requires solution of a moderately large ($N = 100 - 3000$) matrix equation for each zone. Since general solution of a dense matrix scales as $O(N^3)$, this can make these large networks progressively much more expensive. While in principal, every species reacts with each of the hundreds of others, resulting in a dense Jacobian matrix, in practice it is possible to neglect most of these reactions. Because of the $Z_i Z_j$ dependence of the repulsive Coulomb term in the nuclear potential, captures of free neutrons and isotopes of H and He on heavy nuclei occur much faster than fusions of heavier nuclei. Furthermore, with the exception of the Big Bang nucleosynthesis and PP-chains, reactions involving secondary isotopes of H (deuterium and tritium) and He are neglectable. Likewise, photodisintegrations tend to eject free nucleons or α -particles. Thus, with a few important exceptions, for each nucleus we need only consider twelve reactions linking it to its nuclear neighbors by the capture of an n, p, α or γ and release a different one of these four. The exceptions to this rule are the few heavy ion reactions important for burning stages like carbon and oxy-

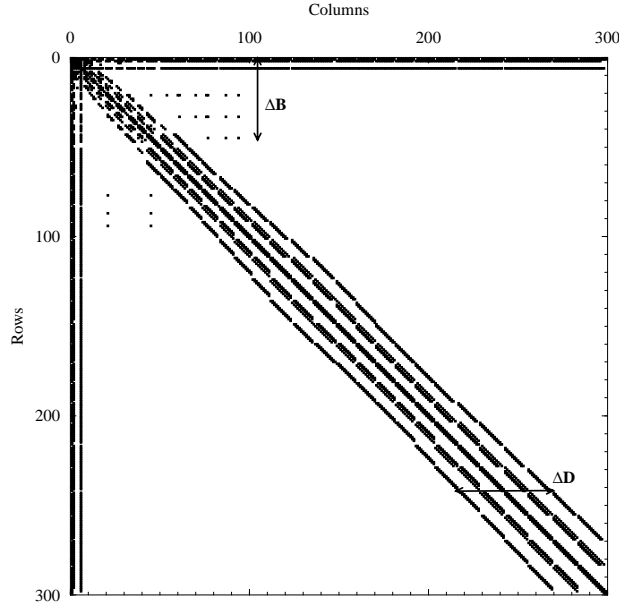


Fig. 1. Graphic demonstration of the sparseness of the Jacobian matrix. The filled squares represent the non-zero elements.

gen burning where the dearth of light nuclei cause the heavy ion collisions to dominate.

Fig. 1 demonstrates the sparseness of the resulting Jacobian matrix, for a 300 nuclei network chosen to handle all the energy generating stages in the life of a massive star. The nuclei are indexed in order of increasing Z and then A . Of the 90,000 matrix elements, fewer than 5,000 are non-zero. In terms of the standard forms for sparse matrices, this Jacobian is best described as doubly bordered, band diagonal. With a border width, ΔB , of 45 necessary to include the heavy ion reactions among ^{12}C , ^{16}O and ^{20}Ne along with the free neutrons, protons and α -particles and a band diagonal width, ΔD , of 54, even this sparse form includes almost 50,000 elements. With solution of the matrix equation consuming 90+% of the computational time, there is clearly a need for custom tailored solvers which take better advantage of the sparseness of the Jacobian [43]. To date best results for small ($N < 100$) matrices are obtained with machine optimized dense solvers (e.g. LAPACK) or matrix specific solvers generated by symbolic processing [41,44]. For large matrices, generalized sparse solvers, both custom built and from software libraries, are used (see, [58]).

Thus far in this section we have considered thermonuclear kinetics in the limit where the hydrodynamics is treated separately by operator-splitting. However, as we discussed in §2.3, this approach is not always viable, so we conclude this section with some remarks on the additional challenges encountered in recent efforts to solve coupled nucleosynthesis and hydrodynamical

mixing. Because these calculations must also be finite differenced with an implicit scheme, they too require matrix solutions and all zones must be solved concurrently. The resulting matrices are quite large: without consideration of matrix sparseness, one would need to store $N^2 M^2$ numbers, where N is the number of species in each zone and M is the number of zones. Fortunately, however, the resulting matrices are quite sparse since they are block diagonal (each block is similar in form to that shown in Fig. 1) with bands linking adjacent spatial zones. Such large sparse matrices are typically solved by iterative techniques, such as biconjugate gradient which requires only matrix multiplies and, thus, only storage of the non-zero matrix elements. To date, computation of $N = 1000$, $M = 1000$ problems (that is, $10^6 \times 10^6$ matrices) can be fairly routinely handled on a single processor. This approach to solving coupled nucleosynthesis and nuclear mixing is necessary in cases where operator splitting is suspect, and we expect to see it finding greater use in future calculations.

3.2 Physically Motivated Network Specialization

Often from a physical understanding one can specialize the general solution method and thereby greatly reduce the computational cost. As an example, we briefly discuss the r-process approximation described in [63,64]. For nuclei with $A > 100$, charged particle captures (proton and α) as well as their reverse photodisintegrations virtually cease when $T < 3$ GK. This leaves only neutron captures and their reverse photodisintegration reactions, as well as β -decays, which can also lead to the emission of delayed neutrons. In this case, Eq. 10 greatly simplifies, leaving

$$\begin{aligned} \dot{Y}({}^A Z) = & n_n \langle \sigma v \rangle_{Z,A-1}^{n,\gamma} Y({}^{A-1} Z) + \lambda_{Z,A+1}^\gamma Y({}^{A+1} Z) + \sum_{j=0}^J \lambda_{Z-1,A+j}^{\beta j n} Y({}^{A+j} Z - 1) \\ & - \left(n_n \langle \sigma v \rangle_{Z,A}^{n,\gamma} + \lambda_{Z,A}^\gamma + \sum_{j=0}^J \lambda_{Z,A}^{\beta j n} \right) Y({}^A Z) , \end{aligned} \quad (20)$$

where $\langle \sigma v \rangle_{Z,A}^{n,\gamma}$ and $\lambda_{Z,A}^\gamma$ are the velocity integrated neutron capture cross section and the photodisintegration rate for the nucleus ${}^A Z$, while $\lambda_{(Z,A)}^{\beta j n}$ is the decay constant for the β^- decay of ${}^A Z$, with j delayed neutrons (up to a maximum of J). The assumption is made that the neutron abundance ($Y_n = n_n / \rho N_A$) varies slowly enough that it may be evolved explicitly. One can see that in Eq. 20, with n_n thereby fixed, the time derivatives of each species have a linear dependence on only the abundances of their neighbors in the same isotopic chain (nuclei with the same Z), or that with one less proton ($Z - 1$). One can then divide the network into separate pieces for each isotopic chain, and solve them sequentially, beginning with the lowest Z . The “boundary” terms for this

lowest Z chain can be supplied by a previously run or concurrently running full network calculation which need extend only to this Z . This reduces the solution of a matrix with more than a thousand rows to the solution of roughly 30 smaller matrices. Furthermore each of these smaller matrices is also tridiagonal increasing speed further. Freiburghaus et al. [64] tested the assumption of slow variation in the neutron abundance and have demonstrated the usefulness of this method in r-process simulations, achieving a large decrease in computational cost. A similar treatment has been successfully applied to explosive hydrogen burning based on the assumption of slowly varying proton and alpha abundances [65]. As we will discuss in §5, for other burning stages there also exist physically motivated simplifications to the general network solution method.

4 Equilibria in Nuclear Astrophysics

An isolated thermodynamic system tends to evolve towards an equilibrium state, and whether the system reaches that equilibrium depends on the competition between the timescale for equilibration and the other relevant timescales. For example, the reaction-rate expression found in Eq. (5) assumed a local thermal equilibrium in the plasma such that the velocities of the interacting particles are well described by a Maxwell-Boltzmann distribution, which is determined by a single parameter, the local temperature. This is valid because the timescale to achieve this equilibrium is much shorter than the other interaction timescales in the plasma. Similarly, as discussed in §2.1, it is usually assumed in nuclear astrophysics that the internal states of a nucleus are also in equilibrium so that the probability of finding a nucleus in particular excited state is proportional to the Boltzmann factor for that state, which, as before, is determined by the temperature and the (presumably known) excitation energy of the state. Again this is generally a valid assumption because the transitions within the nucleus are typically much faster than other interactions, although interesting challenges arise when this assumption is not valid (e.g., [29,30]).

At conditions of high temperature and density, the thermonuclear reaction rates themselves may be sufficiently rapid to achieve equilibrium within the timescale set by the hydrodynamics of the astrophysical setting. This permits considerable simplification of the calculation of the nuclear abundances. In most such cases, the fast strong and electromagnetic reactions reach equilibrium while those involving the weak nuclear force do not. Since the weak reactions are not equilibrated, the resulting *Nuclear Statistical Equilibrium* (NSE) requires monitoring of weak reaction activity. Even with this stricture, NSE offers many advantages, since hundreds of abundances are uniquely defined by the thermodynamic conditions and a single measure of the weak interaction history or the degree of neutronization. Computationally, this reduction

in the number of independent variables greatly reduces the cost of nuclear abundance evolution. Because there are fewer variables to follow within a hydrodynamic model, the memory footprint of the nuclear abundances is also reduced, an issue of importance in modern multi-dimensional models. Finally, the equilibrium abundance calculations depend on binding energies and partition functions, quantities which are better known than many reaction rates. This is particularly true for unstable nuclei and for conditions where the mass density approaches that of the nucleus itself, resulting in exotic nuclear structures.

The expression for NSE is commonly derived using either chemical potentials or detailed balance (see, e.g., [3]). For a nucleus AZ , composed of Z protons and $N = (A - Z)$ neutrons, in equilibrium with these free nucleons, the chemical potential of AZ can be expressed in terms of the chemical potentials of the free nucleons

$$\mu_{Z,A} = Z\mu_p + N\mu_n. \quad (21)$$

Substituting the expression for the Boltzmann chemical potential (including rest mass) into Eq. 21 allows derivation of an expression for the abundance of every nuclear species in terms of the abundances of the free protons (Y_p) and neutrons (Y_n),

$$Y({}^AZ) = \frac{G({}^AZ)}{2^A} \left(\frac{\rho N_A}{\theta} \right)^{A-1} A^{\frac{3}{2}} \exp \left(\frac{B({}^AZ)}{k_B T} \right) Y_n^N Y_p^Z, \quad (22)$$

where $G({}^AZ)$ and $B({}^AZ)$ are the partition function and binding energy of the nucleus AZ , N_A is Avagadro's number, k_B is Boltzmann's constant, ρ and T are the density and temperature of the plasma, and $\theta = (m_u k_B T / 2\pi \hbar^2)^{3/2}$.

Abundances of all nuclear species can therefore be expressed as functions of two quantities. Nucleon number conservation ($\sum AY = 1$) provides one constraint. The second constraint is the amount of weak reaction activity, often expressed in terms of the total proton abundance, $\sum ZY$, which charge conservation requires equal the electron abundance, Y_e . Thus the nuclear abundances are uniquely determined for a given (T, ρ, Y_e) . Alternately, the weak interaction history is sometimes expressed in terms of the neutron excess $\eta = \sum (N - Z)Y$. Figure 2 displays the temperature and density dependence of $\bar{A} = \sum AY / \sum Y = 1 / \sum Y$, the average nuclear mass of the NSE distribution. At high temperatures, free nucleons are favored, hence $\bar{A} \sim 1$. For intermediate temperatures the compromise of retaining large numbers of particles while increasing binding energy favors ${}^4\text{He}$, which has 80% of the binding energy of the iron peak nuclei. At low temperatures, Eq. 22 strongly favors the most bound nuclei, the iron peak nuclei, so $\bar{A} \rightarrow 60$ as the temperature drops. Density can

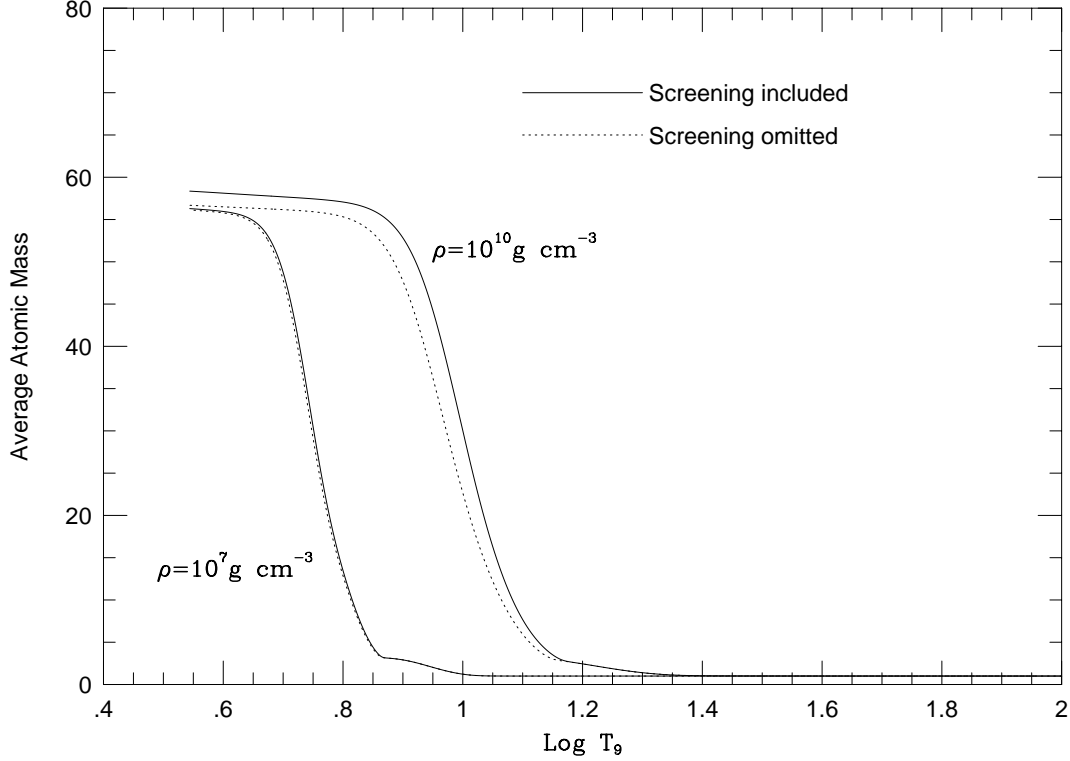


Fig. 2. The average atomic mass for material in NSE as a function of Temperature. The solid lines include screening corrections to the nuclear binding energies, while the dotted lines ignore this effect.

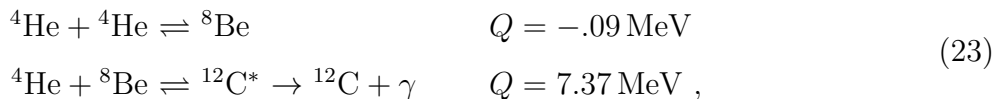
be seen to scale the placement of these divisions between high, intermediate and low temperature and increase the average mass at low temperature. Variations in Y_e do not strongly affect Figure 2. At high temperatures, it simply effects the ratio of $Y_p/Y_n \approx Y_e/1 - Y_e$. At low temperatures, variation in Y_e changes which Fe-peak isotopes dominate. For example, though ^{56}Ni is less tightly bound than ^{54}Fe , it is more tightly bound than $^{54}\text{Fe} + 2\ ^1\text{H}$, which would be required by charge conservation if $Y_e \sim .5$. Thus $Y(^{56}\text{Ni}) > Y(^{54}\text{Fe})$ for low T with $Y_e \sim .50$, but $Y(^{54}\text{Fe}) > Y(^{56}\text{Ni})$ for smaller Y_e . In general, the most abundant nuclei at low temperatures are the most bound nuclei for which $Z/A \sim Y_e$.

As with any equilibrium distribution, there are limitations on the applicability of NSE. For NSE to provide a good estimate of the nuclear abundances the temperature must be sufficient for the endoergic reaction of each reaction pair to occur. Since for all particle-stable nuclei between the proton and neutron drip lines (with the exception of nuclei unstable against alpha decay), the photodisintegrations are endoergic, with typical Q-values among (β) stable nuclei of 8-12 MeV, by Eq. 7 this requirement reduces to $T > 3\text{ GK}$. While this requirement is necessary, it is not sufficient. In the case of hydrostatic silicon burning, even when this condition is met, appreciable time is required to convert Si to Fe-peak elements. In the case of explosive silicon burning,

the adiabatic cooling on timescales of seconds can cause conditions to change more rapidly than NSE can follow, breaking down NSE first between ${}^4\text{He}$ and ${}^{12}\text{C}$, at $T \sim 6\text{ GK}$ [66] and later between the species near silicon and the Fe-peak nuclei, at $T \sim 4\text{ GK}$ [67,68]. Thus it is clear that in the face of sufficiently rapid thermodynamic variations, NSE provides a problematic estimate of abundances. It is important to note that, in spite of the breakdown of the global NSE, many nuclei under these conditions do obey local equilibrium relations with their neighbors.

5 Merging Equilibria with Reaction Networks

In spite of the limitations on the applicability of NSE, the reduced computational cost provides a strong motivation to maximize the use of equilibria. The use of equilibrium expressions for single abundances is, in fact, common in nuclear reaction networks, typically to track the abundances of short-lived unstable intermediates in “three-particle” processes. The most common example of this is the triple α process,



by which Helium burning occurs. With $\tau({}^8\text{Be}) \sim 10^{-16}\text{ sec}$, only rarely does a ${}^8\text{Be}$ survive long enough for a second α to capture. As a result of the near balance of the first reaction pair, the abundance of ${}^8\text{Be}$ can be expressed in terms of the α -particle abundance,

$$Y({}^8\text{Be}) = \frac{\rho N_A}{\theta} \left(\frac{1}{2}\right)^{3/2} \exp\left(\frac{M({}^8\text{Be}) - 2M_\alpha}{k_B T}\right) Y_\alpha^2. \quad (24)$$

Likewise for temperatures in excess of .1 GK, the most likely result following the second α capture to form an excited state of ${}^{12}\text{C}$ is a decay back to ${}^8\text{Be}$ ($\Gamma_\alpha({}^{12}\text{C}^*)/\Gamma_\gamma({}^{12}\text{C}^*) > 10^3$), thus the abundance of ${}^{12}\text{C}^*$ is well characterized by

$$Y({}^{12}\text{C}^*) = \left(\frac{\rho N_A}{\theta}\right)^2 \left(\frac{3}{16}\right)^{3/2} \exp\left(\frac{M({}^{12}\text{C}^*) - 3M_\alpha}{k_B T}\right) Y_\alpha^3. \quad (25)$$

When this is the case, the effective triple α reaction rate is simply that of the decay of ${}^{12}\text{C}$ from the excited state to the ground state,

$$r_{3\alpha} = \rho N_A Y({}^{12}\text{C}^*) \Gamma_\gamma({}^{12}\text{C}^*)/\hbar. \quad (26)$$

This use of local equilibrium within a rate equation shares many characteristics with the more elaborate schemes we will discuss next. The number of species tracked by the network is reduced since $Y(^8\text{Be})$ need not be directly evolved. Problematically small timescales like $\tau(^8\text{Be})$ are removed, replaced by larger time scales ($\tau_{3\alpha} \sim 10^5 - 10^7$ years during core helium burning). The non-linearity of network time derivatives is increased ($\dot{Y}(^{12}\text{C}) \propto Y_\alpha^3$) under this scheme. This approximation also breaks down at low T (for details see [39]).

6 The QSE-reduced Network

As we noted in the previous section, while global NSE may not always apply for temperatures in the range 3-6 GK, many nuclei are in local equilibrium with their neighbors. Beginning with Bodansky et al. [69], a number of attempts have been made to take advantage of these partial equilibria (termed quasi-equilibria or QSE) to reduce the number of independent variables evolved via rate equations and thereby reduce the computational cost of modeling these burning stages. To evolve the abundances of every member of a QSE group, it is sufficient to evolve the abundance of any single group member along with the abundances of the free nucleons. One can thereby reduce the number of abundances that are evolved, while still calculating, from QSE relations, the abundances of all members of a QSE group and the resultant reaction rates, including the electron and neutrino capture reactions responsible for changes in the neutronization. The result is a more computationally efficient method that retains the accuracy of the full network and yields abundances for all nuclei found in the full network. Such methods have been applied to the α -network and produced networks that are twice as fast as the minimal α -chain network, without significantly affecting the nuclear evolution [70,71]. Reductions of an order of magnitude in computational cost have been achieved [72,73] for QSE-reduced networks of the size necessary to capture the essential features of supernova nucleosynthesis and we believe greater savings are possible with further refinement. In addition to silicon burning, there are a number of astrophysically important situations where $T > Q/30k_B$ for at least some of the relevant reactions and so large equilibrium groups exist, but NSE is not globally valid. This includes the r-process [63] and the rp-process in X-ray bursts (and possibly novae) [65], where neutron or proton separation energies (Q_n or Q_p) of 2 MeV and less are often encountered.

As an example, we will discuss the QSE-reduced α -network. Its mission is to evolve the abundances of the full 14 elements of a conventional α -network (which we'll call $\vec{Y}^{\mathcal{F}}$), and calculate the resulting energy generation, in a more efficient way. Under conditions where QSE applies, the existence of the silicon and iron peak QSE groups (which are separated by the nuclear shell closures $Z=N=20$ and the resulting small Q -values and reaction rates) allows calcu-

lation of these 14 abundances from 7. For the members of the silicon group (^{28}Si , ^{32}S , ^{36}Ar , ^{40}Ca , ^{44}Ti) and the iron peak group (^{48}Cr , ^{52}Fe , ^{56}Ni , ^{60}Zn) the individual abundances can be calculated by expressions similar to Eq. 22,

$$\begin{aligned} Y_{QSE,\text{Si}}(^A Z) &= \frac{C(^A Z)}{C(^{28}\text{Si})} Y(^{28}\text{Si}) Y_\alpha^{\frac{A-28}{4}} \\ Y_{QSE,\text{Ni}}(^A Z) &= \frac{C(^A Z)}{C(^{56}\text{Ni})} Y(^{56}\text{Ni}) Y_\alpha^{\frac{A-56}{4}}, \end{aligned} \quad (27)$$

where $C(^A Z)$ is defined in Eq. 22 and $(A-28)/4$ and $(A-56)/4$ are the number of α -particles needed to construct $^A Z$ from ^{28}Si and ^{56}Ni , respectively. Where QSE applies, $\vec{Y}^{\mathcal{F}}$ is a function of the abundances of a reduced nuclear set, \mathcal{R} , defined as α , ^{12}C , ^{16}O , ^{20}Ne , ^{24}Mg , ^{28}Si , ^{56}Ni and we need only evolve $\vec{Y}^{\mathcal{R}}$. It should be noted that ^{24}Mg is ordinarily a member of the silicon QSE group [5,67,74], but for easier integration of prior burning stages with a conventional nuclear network, we will evolve ^{24}Mg independently. The main task when applying such hybrid schemes is finding the boundaries of QSE groups and where individual nuclei have to be used instead. Treating marginal group members as part of a group increases the efficiency of the calculation, but may decrease the accuracy.

While $\vec{Y}^{\mathcal{R}}$ is a convenient set of abundances for calculating $\vec{Y}^{\mathcal{F}}$, it is not the most efficient set to evolve, primarily because of the non-linear dependence on Y_α . Instead we define a set of group abundances, $\vec{Y}^{\mathcal{G}} = [Y_{\alpha G}, Y(^{12}\text{C}), Y(^{16}\text{O}), Y(^{20}\text{Ne}), Y(^{24}\text{Mg}), Y_{SiG}, Y_{FeG}]$ where

$$\begin{aligned} Y_{\alpha G} &= Y_\alpha + \sum_{i \in \text{Si group}} \frac{A_i - 28}{4} Y_i + \sum_{i \in \text{Fe group}} \frac{A_i - 56}{4} Y_i, \\ Y_{SiG} &= \sum_{i \in \text{Si group}} Y_i, \\ Y_{FeG} &= \sum_{i \in \text{Fe group}} Y_i. \end{aligned} \quad (28)$$

Physically, $Y_{\alpha G}$ represents the sum of the abundances of free α -particles and those α -particles required to build the members of the QSE groups from ^{28}Si or ^{56}Ni , while Y_{SiG} and Y_{FeG} represent the total abundances of the silicon and iron peak QSE groups. This method, which here is applied only to the chain of α -nuclei can also be generalized to arbitrary networks [73]. For larger networks which contain nuclei with $N \neq Z$, one must be able to follow the abundances of free neutrons and protons, particularly since weak interactions will change the global ratio of neutrons to protons. In place of $Y_{\alpha G}$ in Eq. 28, one constructs $Y_{NG} = \sum_{i, \text{light}} N_i Y_i + \sum_{i, \text{Si}} (N_i - 14) Y_i + \sum_{i, \text{Fe}} (N_i - 28) Y_i$ and $Y_{ZG} = \sum_{i, \text{light}} Z_i Y_i + \sum_{i, \text{Si}} (Z_i - 14) Y_i + \sum_{i, \text{Fe}} (Z_i - 28) Y_i$, if ^{28}Si and ^{56}Ni are chosen as the focal nuclei for the Si and Fe groups.

Corresponding to this reduced set of abundances \mathcal{G} is a reduced set of reactions, with quasi-equilibrium allowing one to ignore the reactions among the members of the QSE groups. Unfortunately, the rates of these remaining reactions are functions of the full abundance set, $\vec{Y}^{\mathcal{F}}$, and are not easily expressed in terms of the group abundances, $\vec{Y}^{\mathcal{G}}$. Thus, for each $\vec{Y}^{\mathcal{G}}$, one must solve for $\vec{Y}^{\mathcal{R}}$ and, by Eq. 27, $\vec{Y}^{\mathcal{F}}$, in order to calculate $\dot{\vec{Y}}^{\mathcal{G}}$ which is needed to evolve $\vec{Y}^{\mathcal{G}}$ via Eq. 16. Furthermore, Eq. 18 requires the calculation of the Jacobian of $\dot{\vec{Z}}$, which can not be calculated directly since $\dot{\vec{Y}}^{\mathcal{G}}$ cannot be expressed in terms of $\vec{Y}^{\mathcal{G}}$. Instead it is sufficient to use the chain rule,

$$\frac{\partial \dot{\vec{Y}}^{\mathcal{G}}}{\partial \vec{Y}^{\mathcal{G}}} = \frac{\partial \dot{\vec{Y}}^{\mathcal{G}}}{\partial \vec{Y}^{\mathcal{R}}} \frac{\partial \vec{Y}^{\mathcal{R}}}{\partial \vec{Y}^{\mathcal{G}}} \quad (29)$$

to calculate the Jacobian. Analytically, the first term of the chain rule product is easily calculated from the sums of reaction terms, while the second term requires implicit differentiation using Eq. 28. Additional details and comparisons with the full α -network are demonstrated by Hix et al. [70] (See also [71]).

7 Conclusion

Computational astrophysics is in the midst of a paradigm shift. For many years, one dimensional Lagrangian models, which take advantage of the (near) sphericity of self-gravitating fluids, have been the standard for modeling the lives, deaths and afterlives of stars. Increasingly, we see these models being supplanted by multi-dimensional models which can more accurately include the wide variety of phenomena which break spherical symmetry (for example, rotation, convection and/or magnetic fields). Present day computational capability limits the use of such multi-dimensional models to short-lived episodes in the stellar life cycle, but the future will see increasing usage of such models. An important limitation of the current multi-dimensional models is the small number of nuclear species which are evolved within these models, typically less than twenty. This is in contrast to the hundreds or thousands of species tracked in the one dimensional models. Removing this limitation is vital if we are to continue to compare models to the myriad of observations which reveal the elemental and isotopic composition of the Universe. This will require continued improvements in the numerical methods we have discussed.

In this article, we have reviewed the numerical methods presently used to study thermonuclear kinetics in astrophysics and highlighted the directions in which we see promise for improvements in speed and accuracy. Nuclear compositions are currently evolved within astrophysical simulations via ther-

monuclear rate equations or Nuclear Statistical Equilibrium. While NSE solutions are much more economical, principally because of the much smaller number of free parameters that must be evolved, they are applicable to only a few situations. The principle difficulty with evolution via rate equation is the computational cost, which results primarily from the stiffness of the system of nuclear reactions. This extreme stiffness requires implicit solution and has thus far generally precluded the use of integration methods that do not rely on the Jacobian matrix. Such non-Jacobian methods remain highly sought after as a means to reduce the computational cost of nucleosynthesis calculations. For Jacobian based integration methods, there remain considerable economies to be gained by taking better advantage of the sparse nature of the Jacobian and by reuse of the inverted Jacobian.

Physically motivated approaches can also be extremely useful in reducing the computational cost. One such is the use of local equilibria to reduce the size of the system of rate equations (and reduce problems with matrix singularity). Methods based on local equilibria are applicable to many situations where global equilibrium has not been achieved. Though the use of hybrid equilibrium networks is in its infancy, it seems that in many of the situations where one would have heretofore used a large network coupled with hydrodynamics, the hybrid equilibrium networks provide sufficient accuracy and considerable reduction in the computational cost. Ultimately, both physically inspired and computationally motivated improvements will be necessary as we strive to extend the reach of multi-dimensional simulations.

Acknowledgements

As a review, this article naturally owes much to the innumerable investigators who have devoted at least part of their life's work to our understanding of nucleosynthesis in astrophysical environments. The authors would like to specifically thank W.D. Arnett, G. Bazan, A.G.W. Cameron, E. Müller, K. Nomoto, T. Plewa, F.-K. Thielemann and S.E. Woosley who were especially influential in the preparation of this review. Comments from the referee, F.X. Timmes, were particularly helpful. The work has been partly supported by the National Science Foundation under contracts AST-9877130, AST-9819877, and PHY-0244783, by the Department of Energy, through the Scientific Discovery through Advanced Computing Programs, and by funds from the Joint Institute for Heavy Ion Research at ORNL. Oak Ridge National Laboratory is managed by UT-Battelle, LLC, for the U.S. Department of Energy under contract DE-AC05-00OR22725.

References

- [1] E. M. Burbidge, G. R. Burbidge, W. A. Fowler, F. Hoyle, *Rev. Mod. Phys.* 29 (1957) 547–650.
- [2] A. G. W. Cameron, *PASP* 69 (1957) 201–222, atomic Energy of Canada, Ltd., CRL-41.
- [3] D. D. Clayton, *Principles of Stellar Evolution and Nucleosynthesis*, Chicago: University of Chicago Press, 1983.
- [4] C. Rolfs, W. Rodney, *Cauldrons in the Cosmos*, Chicago: Univ. of Chicago, 1988.
- [5] W. D. Arnett, *Supernovae and nucleosynthesis : an investigation of the history of matter, from the big bang to the present*, Princeton University Press, Princeton, 1996.
- [6] W. Fowler, G. Caughlan, B. Zimmermann, *ARA&A* 5 (1967) 525.
- [7] F. Käppeler, F.-K. Thielemann, M. Wiescher, *Annu. Rev. Nucl. Part. Sci.* 48 (1998) 175–251.
- [8] W. Haxton, P. Parker, C. Rolfs, *Nucl. Phys. A* This volume.
- [9] L. Buchmann, C. Barnes, *Nucl. Phys. A* This volume.
- [10] C. Angulo, A. Shotter, J. Blackmon, *Nucl. Phys. A* This volume.
- [11] A. Hernanz, J. Jose, C. Iliadis, *Nucl. Phys. A* This volume.
- [12] E. Rehm, H. Schatz, *Nucl. Phys. A* This volume.
- [13] F. Kaeppler, A. Mengoni, *Nucl. Phys. A* This volume.
- [14] H. Geissel, K.-L. Kratz, B. Sherill, *Nucl. Phys. A* This volume.
- [15] T. Rauscher, P. Descouvemont, *Nucl. Phys. A* This volume.
- [16] L. Marcucci, K. Nollett, B. Wiringa, *Nucl. Phys. A* This volume.
- [17] G. R. Caughlan, W. A. Fowler, *At. Data Nuc. Data Tab.* 40 (1988) 283.
- [18] S. Goriely, M. Rayet, M. Samyn, P. Demetriou, A. Jorissen, M. Arnould, *Nucl. Phys. A* This volume.
- [19] M. S. Smith, *Nucl. Phys. A* 718 (2003) 339–346.
- [20] P. Mohr, A. Zilges, Utsonomi, *Nucl. Phys. A* This volume.
- [21] E. E. Salpeter, *Australian Journal of Physics* 7 (1954) 373.
- [22] H. E. Dewitt, H. C. Graboske, M. S. Cooper, *ApJ* 181 (1973) 439–456.
- [23] S. Ichimaru, *Reviews of Modern Physics* 65 (1993) 255–299.

- [24] L. S. Brown, R. F. Sawyer, *Rev. Mod. Phys.* 69 (1997) 411–436.
- [25] E. E. Salpeter, H. M. van Horn, *ApJ* 155 (1969) 183.
- [26] S. Ichimaru, H. Kitamura, *Physics of Plasmas* 6 (1999) 2649–2671.
- [27] T. Rauscher, F. Thielemann, *At. Data Nuc. Data Tab.* 75 (2000) 1–2.
- [28] C. Angulo, M. Arnould, M. Rayet, P. Descouvemont, D. Baye, C. Leclercq-Willain, A. Coc, S. Barhoumi, P. Aguer, C. Rolfs, R. Kunz, J. W. Hammer, A. Mayer, T. Paradellis, S. Kossionides, C. Chronidou, K. Spyrou, S. degl’Innocenti, G. Fiorentini, B. Ricci, S. Zavatarelli, C. Providencia, H. Wolters, J. Soares, C. Grama, J. Rahighi, A. Shotter, M. Lamahi Rachti, *Nucl. Phys. A* 656 (1999) 3–183.
- [29] R. A. Ward, W. A. Fowler, *ApJ* 238 (1980) 266–286.
- [30] S. S. Gupta, B. S. Meyer, *Phys. Rev. C* 64 (2001) 025805.
- [31] M. Liebendoerfer, G. Martinez-Pinedo, D. Frekers, *Nucl. Phys. A* This volume.
- [32] I. Borzov, *Nucl. Phys. A* This volume.
- [33] K. Takahashi, F. Bosch, T. Faestermann, P. Kienle, *Nucl. Phys. A* This volume.
- [34] G. M. Fuller, B. S. Meyer, *ApJ* 453 (1995) 792.
- [35] A. Burrows, S. Reddy, *Nucl. Phys. A* This volume.
- [36] G. Fuller, G. Raffelt, *Nucl. Phys. A* This volume.
- [37] P. Vogel, *Nucl. Phys. A* This volume.
- [38] A. Mezzacappa, O. E. B. Messer, *J. Comp. Appl. Math* 109 (1999) 281–319.
- [39] K. Nomoto, F.-K. Thielemann, S. Miyaji, *A&A* 149 (1985) 239–245.
- [40] J. Görres, M. Wiescher, F. Thielemann, *Phys. Rev. C* 51 (1995) 392–400.
- [41] E. Müller, in: *Saas-Fee Advanced Course 27: Computational Methods for Astrophysical Fluid Flow.*, 1998, p. 343.
- [42] G. Audi, A. H. Wapstra, *Nucl. Phys. A* 595 (1995) 409–480.
- [43] N. Prantzos, M. Arnould, J.-P. Arcoragi, *ApJ*, 315 (1987) 209–228
- [44] E. Mueller, *A&A* 162 (1986) 103–108.
- [45] W. Arnett, J. Truran, *ApJ* 157 (1969) 339.
- [46] T. A. Weaver, G. B. Zimmerman, S. E. Woosley, *ApJ* 225 (1978) 1021–1029.
- [47] W. Benz, F.-K. Thielemann, J. G. Hills, *ApJ* 342 (1989) 986–998.
- [48] J. C. Niemeyer, W. Hillebrandt, *ApJ* 452 (1995) 769.
- [49] A. M. Khokhlov, *ApJ* 449 (1995) 695.

- [50] B. Fryxell, E. Müller, W. Arnett, Hydrodynamics and nuclear burning, Tech. rep., Max-Planck-Institut für Astrophysik, Garching, Preprint 449 (1989).
- [51] B. LARROUTUROU, J. Comp. Phys. 95 (1991) 59–84.
- [52] T. Plewa, E. Müller, A&A 342 (1999) 179–191.
- [53] G. Bazan, D. Arnett, ApJ 496 (1998) 316.
- [54] C. Gear, Numerical Initial Value Problems in Ordinary Differential Equations, Prentice-Hall, Englewood Cliffs, NJ, 1971.
- [55] J. Lambert, in: I. Gladwell, D. Sayars (Eds.), Computational Techniques for Ordinary Differential Equations, Academic Press, New York, 1980, pp. 19–46.
- [56] E. Oran, J. Boris, Numerical Simulation of Reactive Flow, 2nd Edition, Cambridge University Press, Cambridge, 2001.
- [57] B. Fields, K. Olive, Nucl. Phys. A This volume.
- [58] F. X. Timmes, ApJS 124 (1999) 241–263.
- [59] D. Mott, E. Oran, van Leer B., J. Comp. Phys. 164 (2000) 407–428.
- [60] R. V. Wagoner, ApJ 179 (1973) 343–360.
- [61] W. Press, S. Teukolsky, W. Vetterling, B. Flannery, Numerical Recipes, (Cambridge:Cambridge Univ.), 1992, second edition.
- [62] A. Khokhlov, Yass - yet another stiff solver that works., Tech. rep., NRL Technical Memorandum Report.
- [63] J. J. Cowan, F. Thielemann, J. W. Truran, ARA&A 29 (1991) 447–497.
- [64] C. Freiburghaus, J.-F. Rembges, T. Rauscher, E. Kolbe, F.-K. Thielemann, K.-L. Kratz, B. Pfeiffer, J. J. Cowan, ApJ 516 (1999) 381–398.
- [65] F. Rembges, C. Freiburghaus, T. Rauscher, F.-K. Thielemann, H. Schatz, M. Wiescher, ApJ 484 (1997) 412.
- [66] B. S. Meyer, T. D. Krishnan, D. D. Clayton, ApJ 498 (1998) 808.
- [67] S. E. Woosley, W. D. Arnett, D. D. Clayton, ApJS 26 (1973) 231.
- [68] W. R. Hix, F.-K. Thielemann, ApJ 511 (1999) 862–875.
- [69] D. Bodansky, D. Clayton, W. Fowler, ApJS 16 (1968) 299.
- [70] W. R. Hix, A. M. Khokhlov, J. C. Wheeler, F.-K. Thielemann, ApJ 503 (1998) 332–343.
- [71] F. X. Timmes, R. D. Hoffman, S. E. Woosley, ApJS 129 (2000) 377–398.
- [72] C. Freiburghaus, W. R. Hix, F.-K. Thielemann, in: N. Prantzos (Ed.), Proceeding of Nuclei in the Cosmos V, Paris:Editions Frontiere, 1999, p. 140.
- [73] W. R. Hix, C. Freiburghaus, F.-K. Thielemann, ApJS, In preparation.
- [74] W. R. Hix, F.-K. Thielemann, ApJ 460 (1996) 869–894.